Journal Pre-proof

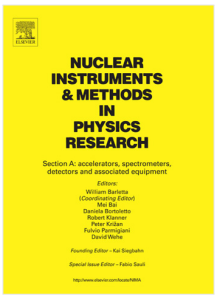

Characterization of scintillating materials in use for brachytherapy fiber based dosimeters

S. Cometti, A. Gierej, A. Giaz, S. Lomazzi, T. Baghdasaryan, J. Van Erps, F. Berghmans, R. Santoro, M. Caccia, S. O'Keeffe

PII: S0168-9002(22)00495-8
DOI: https://doi.org/10.1016/j.nima.2022.167083
Reference: NIMA 167083

To appear in: *Nuclear Inst. and Methods in Physics Research, A*

Received date : 10 February 2022
Revised date : 15 May 2022
Accepted date : 3 June 2022

Please cite this article as: S. Cometti, A. Gierej, A. Giaz et al., Characterization of scintillating materials in use for brachytherapy fiber based dosimeters, *Nuclear Inst. and Methods in Physics Research, A* (2022), doi: https://doi.org/10.1016/j.nima.2022.167083.

Characterization of scintillating materials in use for brachytherapy fiber based dosimeters

S. Cometti[a,*], A. Gierej[b], A. Giaz[a], S. Lomazzi[a], T. Baghdasaryan[b], J. Van Erps[b], F. Berghmans[b], R. Santoro[a], M. Caccia[a], S. O'Keeffe[c]

[a] *Università degli Studi dell'Insubria, Dipartimento di Scienza e Alta Tecnologia, via Valleggio 11, Como, Italy*
[b] *Brussels Photonics (B-PHOT), Vrije Universiteit Brussel and Flanders Make, Dept. of Applied Physics and Photonics, Pleinlaan 2, B-1050 Brussels, Belgium*
[c] *Optical Fibre Sensors Research Centre, University of Limerick, Limerick V94 T9PX, Ireland*

Abstract

This paper reports the characterization of two scintillating materials in powder form, Gadox and YVO embedded in a light-activated resin, used in a probe developed for oncological brachytherapy in-vivo dosimetry. The materials were characterized in terms of internal absorption, scintillation decay time, and light yield. The measurement of the optical characteristics highlighted a significant internal absorption at the scintillation light wavelength, with values of 6.5 dB/mm for Gadox and 14.1 dB/mm for YVO.

Measurements of the characteristics scintillation time and of the light yield were performed with a novel method based on single photon counting, profiting from the long decay time of the materials under study. Measurements have been complemented by a two-step simulation with Geant4 to study the energy deposition followed by a ZEMAX OpticStudio® ray tracing to estimate the light collection efficiency. The decay time for scintillating materials were measured to be $\tau_{Gadox} = (458 \pm 3 \pm 3)\,\mu$s and $\tau_{YVO} = (451 \pm 8 \pm 3)\,\mu$s and the estimated values of the light yield are $(7.1 \pm 0.5) \times 10^4$ photon/MeV for Gadox and $(4.8 \pm 0.5) \times 10^4$ photon/MeV for YVO.

Keywords: Brachytherapy, Inorganic scintillators, single photoelectron, SiPM,

*Corresponding author
Email address: agnese.giaz@uninsubria.it (A. Giaz)

Light yield
2010 MSC: 00-01, 99-00

1. Introduction

The ORIGIN project (Optical Fibre Dose Imaging for Adaptive Brachytherapy), supported by the European Commission within the Horizon 2020 framework program, targets the development of a real-time radiation dose imaging and source localization system for brachytherapy treatments. This goal will be accomplished by the development of a novel 16 to 32 optical fiber-based system. The design of the system will be the same for both Low Dose Rate (LDR) and High Dose Rate (HDR) brachytherapy. Two optical fiber radiation sensors have been developed, integrating with different techniques a minimal volume of scintillator ($0.0327\,\mathrm{mm}^3$) in a clear fiber tip, in order to allow point-like measurements of the delivered dose [1], [2], [3]. The baseline scintillators chosen by ORIGIN are Gadox (Gd_2O_2S:Tb) and YVO ($1Y_2O_3$:Eu+$4YVO_4$:Eu) for the LDR and HDR brachytherapy probes, respectively. Two main reasons have driven the choice of these specific materials: first, the emission wavelengths with main peaks at 544 nm (Gadox) and 619 nm (YVO), allowing to filter Cherenkov light and reduce the stem effect, expected to occur at shorter wavelength; second, the availability of the material in fine-grain powder, allowing to mix the scintillator with a light-activated resin for the integration in the fiber tip. Scintillators in the form of fine powder with micrometer particle size have the advantage that they can be rather easily mixed with various liquid media, for example with an epoxy adhesive or other media including organic and inorganic polymers in a powder form. The combination of the scintillator with another substance gives the ability to customize the scintillator to various shapes of interest using specified manufacturing techniques depending on the used medium. The material properties, in terms of decay time (τ) and light yield (LY), were not provided by the producer, and data reported in literature have a wide spread and a significant dependence on the stoichiometry of the product [4]. The luminescence

properties of the commercially available scintillators including Gadox and YVO have been extensively investigated in [3] and the fiber-optic radiation sensors with these inorganic scintillators have been reported by [3], [5], [6], [7], [8], [9], [10]. In addition, the LY is dependent on the powder grain size and the mixture with the host material. Therefore, a characterization campaign was essential to provide relevant information for the design of the light sensor system.

The estimation of the LY of scintillators is commonly based on the photo-electron yield measured with a photomultiplier tube in correspondence to the photo-peak under irradiation with a γ-ray source [11], [12], [13]. However, the γ-ray spectroscopy technique cannot be applied here since, irrespective from the high atomic number, photo-peaks cannot be identified because of internal absorption and light transmission properties of the mixture, introducing a large spread in the light collection process. Thus, a β-source has been used for the irradiation and the measurement of τ and LY have been performed exploiting the single photon counting capability of the Silicon Photomultipliers (SiPMs).

2. Materials and methods

2.1. Scintillating materials

The characteristics of the scintillators, provided by the producer[1], are reported in Table 1.

Table 1: Gadox and YVO powders characteristics.

Material	Grain size $\varnothing$ [μm]	Density ρ [g/cm^3]	Atomic number Z	Emission wavelength λ [nm]
Gadox powder	$\sim 4\,\mu$m	7.5 g/cm^3	60.13	544 nm
YVO powder	$\sim 7\,\mu$m	5.2 g/cm^3	32.10	619 nm

The characterization has been performed on samples containing the Gadox and YVO powders dispersed in the NOA 61 UV-curing liquid polymer adhesive.

[1] Phosphor Technology - https://www.phosphor-technology.com/

The scintillator in the powder form to the adhesive mass-ratio was 3:2, and the mixtures have been deposited in the 5 mm diameter central hole of a set of custom-made PMMA disks. The samples had an outer diameter of 30 mm and their thickness slightly varied from the targeted values of 5, 3, 1 and 0.5 mm, hence the sample's exact thickness was measured using a digital caliper. An exemplary drawing of the specimen geometry is shown in Fig. 1a. During UV photopolymerization, borosilicate coverslip glasses were applied to the bottom of the specimens to prevent leakages of the scintillating mixture. At the end of the photopolymerization process, the glass slides were removed.

2.2. Optical characterization of the scintillating samples

The transmission measurement accounts for both linearly transmitted and diffused light by means of an integrating sphere. The light source employed for the measurements is a broadband Halogen light focused on the measurement port using a plano-convex lens with a focal length of 25 mm positioned above the integrating sphere aperture. During the measurements the specimens were located on the 6 mm diameter aperture of the integrating sphere. The collected light was guided to the spectrum analyzer (AvaSpec2048) by means of multi-mode optical fibres with a large core diameter of 600 μm to maximize light throughput and signal to noise ratio. The setup used for the optical characterization is shown in Fig. 1b.

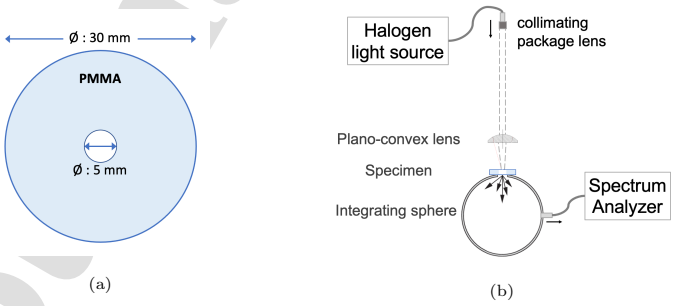

Figure 1: Sketch of the disk hosting the scintillating material in the center (a) and the setup used for the transmission spectroscopy measurement (b).

The collected light was guided to a spectrum analyzer by an optical fiber. The transmittance (T) of the sample has been obtained taking into account the incident and dark spectra recorded before every measurement.

$$T(\lambda) = \frac{I_{sample}(\lambda) - I_{dark}(\lambda)}{I_{incid}(\lambda) - I_{dark}(\lambda)} \quad (1)$$

Fig. 2 shows the transmittance of specimens with various thickness for two mixture types of scintillating materials Gadox and YVO with the NOA61 adhesive. Both materials are characterized by a significant absorption and scattering in the wavelength range corresponding to the given scintillator emission range: i.e., for a 0.55 mm thick specimen, the transmittance is 10.2% for GADOX at 544 nm, and for a 0.57 mm thick specimen, the transmittance is 4.2% for YVO at 619 nm. The transmittance for the thicker samples, i.e., around 3 and 5 mm is close to 0-1% because of their high opacity and limitations of our spectrum analyser. Transmission, linked to attenuation as:

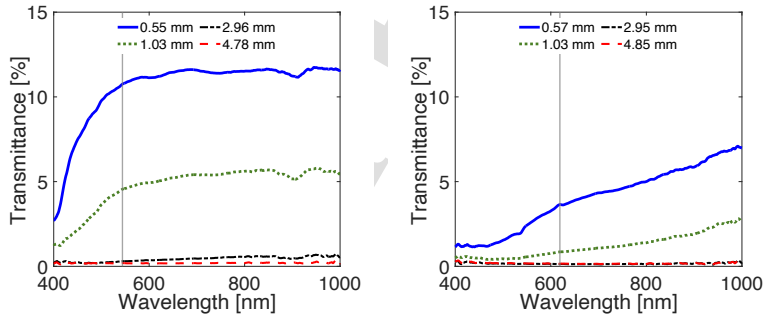

(a) (b)

Figure 2: Transmittance values for Gadox (a) and YVO (b) scintillating mixtures with specimens thickness of 0.5, 1, 3, and 5 mm. The vertical lines represent the wavelengths of the main emission peaks for the two scintillators.

$$A\,[dB] = -10 \cdot log_{10} T \quad (2)$$

was measured at the scintillation wavelength for different thicknesses of the sample (Fig. 3) and the attenuation coefficient α in [db/mm] calculated by the

slope of the linear trend. Measured values correspond to $\alpha_{Gadox} = 6.5\,db/mm$ and $\alpha_{YVO} = 14.1\,db/mm$. It is worth noting that the attenuation coefficient measures the contributions by light absorption and scattering, while reflections are measured by the offset in the linear fit; they are presumed to be the same irrespective from the sample thickness and depends on the refractive indexes of the material under study. The attenuation coefficient can be turned into the penetration length of the Beer-Lambert law $I(x) = I_0 \cdot e^{-x/L}$ as

$$L\,[mm] = \frac{10 \cdot log_{10}\, e}{\alpha} \tag{3}$$

for values of $L_{Gadox} = 0.67mm$ and $L_{YVO} = 0.31\,mm$

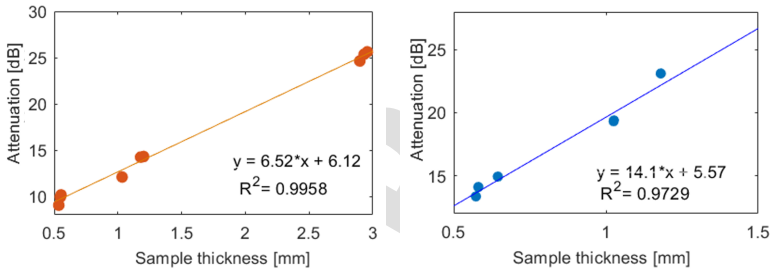

(a) (b)

Figure 3: Attenuation of Gadox (a) and YVO (b) specimens. Dots are the data points and the solid line is the linear regression. The slope returns the attenuation coefficient at 544 nm for Gadox and 619 nm for YVO.

2.3. Estimation of scintillation decay time and light yield

The characterization in terms of scintillating properties has been performed on the thinnest specimens interfaced to a SiPM. The sensor in use was a HAMAMATSU S13360-6050CS SiPM, with the characteristics reported in table 2. Coupling between the sample and the SiPM entrance window was guaranteed interposing an optical grease and, no optical filter was used, during the sample characterization measurements.. Fig. 4 shows the top view of the disk coupled to the SiPM.

Table 2: Main figures of the SiPM in use, the OCT, the DC and the breakdown voltage are measured operating temperature T = 21°C.

Parameter	Description
Effective photosensitive area	$6 \times 6\,\mathrm{mm}^2$
Cell pitch	50 μm
V breakdown (V_{bd})	52.05 ± 0.03 V
V operational (V_{op})	V_{bd} + 3 V
Peak sensitivity length λ_P	450 nm
Photon Detection Efficiency (PDE) $\lambda = \lambda_P$	40 %
Dark Count Rate	1.080 ± 0.001 MHz
Optical Cross Talk	5.5%
After pulsing	∼1%
Gain at V_{op}	$1.7 \cdot 10^6$
Window refractive index (n)	1.41

All the measurements presented in this work heave been performed at constant temperature of 21°C and +3 V over-voltage. The DC, the breakdown voltage and the Optical Cross Talk (OCT) values used in the analysis have been measured, while the PDE was derived from the datasheet values and the after pulsing assumed at the % level according to [14] - [15].

The measurements consisted in recording the scintillation light produced by β-particles interacting with the specimen. The source used for the characterization was ^{90}Sr (produced by Spectrum Techniques[2]) positioned directly over the specimen. The diameter of the sealed source was of 6 mm.

The SiPM signal was amplified, using the PSAU SP5600 by CAEN[3], and then filtered by a pole-zero cancellation circuit (PZC) reducing the pulse dura-

[2]https://www.spectrumtechniques.com/products/sources/
[3]https://www.caen.it/products/sp5600e/

Figure 4: Photo of a 0.5 mm thick specimen coupled to the SiPM.

tion from 300 ns to 30 ns, to enhance the counting rate capability by lowering the single photoelectron (p.e.) pile-up probability. The signal was further amplified in the PSAU before being digitized for the off line analysis, using a CAEN DT5720 digitizer with a sampling rate of 250 MS/s, and 12-bit resolution over a 2 V range. Fig. 5 shows the block diagram of the experimental setup. Since

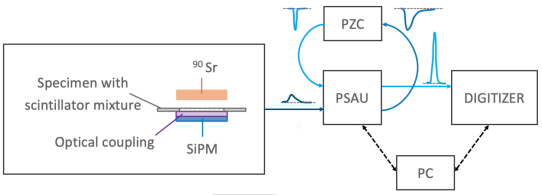

Figure 5: Schematic layout of the experimental setup for the τ and LY measurement.

the expected scintillation decay time is of the order of 0.5 ms [16], [9], the light emitted by an interacting particle generates trails of single p.e. overlayed to Dark Counts (DC), making the identification of the primary events, namely particles crossing the scintillator, not trivial. In our setup, the trigger was based on the prompt signal, with a mean value of 15 p.e., induced in the SiPM by the β particle crossing the specimen and generating charge carriers by ionization in the Silicon substrate [17]. An exemplary event is shown in Fig. 6, where scintillation photons following the direct detection is evident by the Right-Hand Side (RHS).

Data analysis was based on a statistics of 10000 waveforms digitized over

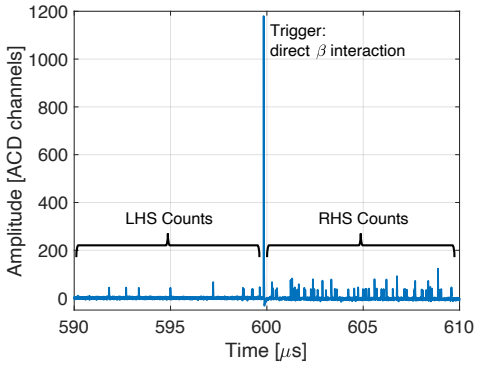

Figure 6: **Exemplary waveform of a Gadox specimen irradiated from the ^{90}Sr source. The main pulse is due to direct detection exploited as trigger followed by the scintillation (RHS Counts). On the left of the main pulse the single p.e. due to the DC (LHS Counts).**

a 1.2 ms window with a trigger at 600 μs. The recorded data were processed subtracting the baseline, identifying and counting the number of p.e. in each peak recorded before and after the trigger. The pulses to the Left-Hand Side (LHS) of the trigger are due to DC and follow a stationary Poisson process, while RHS signal results by a superposition of the DC and the detection of scintillation photons, following a non-homogeneous Poisson process. Waveforms characterized by pile-up of scintillation events have been identified and discarded from the dataset because the superposition of two light emissions in the same 1.2 ms window affect both LHS and RHS distributions. However, the selected datasets were still contaminated by a class of events with no scintillation due to particles crossing only the surrounding PMMA disk. This case is due to the larger acceptance of the SiPM and the extended source core in comparison to the scintillator dimension. For these events the number of pulses in the RHS and LHS gates is expected to be comparable. The event distributions for the two scintillating mixtures are shown in Fig. 7a (Gadox) and Fig. 7b (YVO), where the unbalance between the number of pulses to the RHS and LHS of the trigger

over 600 μs gate for each waveform is displayed.

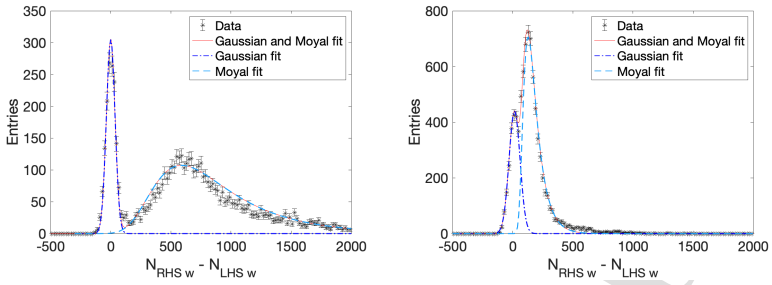

Figure 7: Distribution of $N_{RHS\,W} - N_{LHS\,W}$ fitted with Equation 4. The (a) distribution is referred to a Gadox sample and the (b) distribution to a YVO sample. Both distributions are represented after the rejection of the events that contain scintillation pile-up. The peak around zero was given by the occurrence of events without scintillation emission while the skewed right peak was due to the scintillation event class.

The fraction of the two event classes was estimated fitting these distributions using a superposition of a Gaussian and a Moyal distribution [18], [19]. The former models the class of events with no scintillation, the latter is known to provide a fair approximation of the convolution between a Landau distribution, modeling the energy loss, and a Gaussian function, accounting for detector effects. Equation 4 represents the analytical fitted curve:

$$\frac{W \cdot bin_w \cdot (\mathbf{1\text{-}f})}{\sqrt{2 \cdot \pi} \cdot \sigma_G} \cdot e^{\frac{-(x-\mu_G)^2}{2 \cdot \sigma_G^2}} + \frac{W \cdot bin_w \cdot \mathbf{f}}{\sqrt{2 \cdot \pi} \cdot \sigma_M} \cdot e^{-\frac{1}{2} \cdot e^{-\frac{x-x_P}{\sigma_M}} - \frac{x-\mu_M}{2 \cdot \sigma_M}} \tag{4}$$

where the parameters of the Gaussian distribution (μ_G and σ_G) have been fixed by fitting the distribution $N_{RHS\,W} - N_{LHS\,W}$ of a dataset recorded without radioactive source. The f parameter provides the fraction of scintillation events. Exemplary results of the fitting procedure are shown in Fig. 7a (Gadox) and Fig. 7b (YVO).

As a second step, events in the filtered dataset were processed to provide the average number of pulses in time windows with increasing duration, starting from 10 μs up to 600 μs with 10 μs granularity, as shown in Fig. 8.

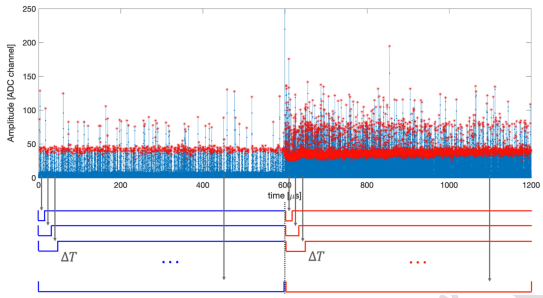

Figure 8: Illustration of the applied method to obtain the average number of pulses in time windows growing with a 10 μs granularity up to 600 μs, both to the LHS and the RHS of the trigger.

The cumulative distribution of the scintillation light against time has been obtained by the difference between the average number of pulses in the RHS ($\langle N^i_{RHS}\rangle$) and the LHS ($\langle N^i_{LHS}\rangle$) bins. For every time window i, counts to the LHS are due to DC only while on the RHS we have both counts due to scintillation and to spurious pulses, namely:

$$\langle N^i_{LHS}\rangle = \langle N^i_{DC}\rangle \tag{5}$$

$$\langle N^i_{RHS}\rangle = (\mathbf{1-f})\cdot\langle N^i_{DC}\rangle + \mathbf{f}\cdot(\langle N^i_{scint}\rangle + \langle N^i_{DC}\rangle) \tag{6}$$

therefore:

$$\langle N^i_{RHS}\rangle - \langle N^i_{LHS}\rangle = \mathbf{f}\cdot\langle N^i_{scint}\rangle \tag{7}$$

The cumulative distribution may be fitted by:

$$N_{tot}(t) = N_0\cdot[1-e^{-t/\tau}] \tag{8}$$

where τ corresponds to the decay time of the scintillator and N_0 is the total number of detected p.e., the asymptote of the cumulative distribution, given by the the effective LY (LY_{eff}) weighted by the fraction of scintillation events: $N_0 = LY_{eff}\cdot f$. Exemplary illustration of the cumulative distributions for the Gadox and YVO are shown in Fig. 9. Measurements have been performed on 3 samples for each scintillating mixture, yielding the following results:

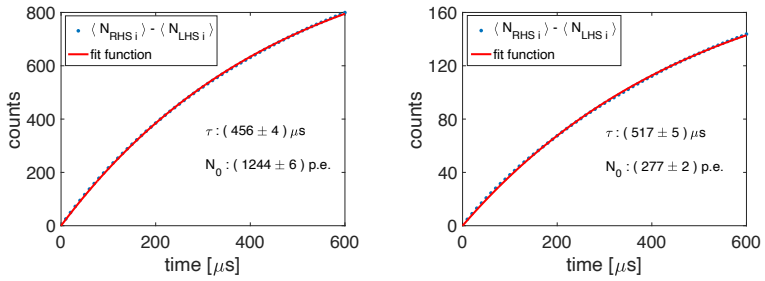

(a) (b)

Figure 9: Fit of the cumulative distributions for the Gadox (a) and YVO (b). The distributions are obtained by the difference between the average number of counted pulses in the RHS and the LHS for each of the sixties time windows.

Gadox mixture	**YVO mixture**
$\tau = (458 \pm 3 \pm 3)\ \mu s$	$\tau = (514 \pm 8 \pm 3)\ \mu s$
$\mathrm{LY}_{eff} = (1384 \pm 59 \pm 21)$ p.e.	$\mathrm{LY}_{eff} = (358 \pm 4 \pm 7)$ p.e.

where the first error is the statistical uncertainty obtained by the cumulative distribution fit of the three samples and the second is a systematic error obtained by the quadrature of the error due to re-positioning and the error due to the sample-to-sample variation.

3. Numerical simulation and LY measurement

The estimated τ values have a general validity while the measured LY_{eff} is specific of the set-up and the specimen characteristics. Beside the properties of the scintillating mixture, geometry does matter, together with interfaces between neighbouring layers, and the sensor PDE at the wavelength of interest. Therefore, to obtain the number of generated photons per unit deposited energy (LY) from the LY_{eff}, the PDE of the SiPM in use has to be considered, together with the evaluation of deposited energy in the scintillator and the effects related to the propagation of the emitted light. The PDE values were estimated

by the convolution of the emission spectra of the two scintillating materials from reference [3] - [20] and the PDE as a function of the wavelength of the SiPM in use. The resulting values from the two scintillators are: $\mathrm{PDE}_{Gadox} = 34\%$ and $\mathrm{PDE}_{YVO} = 25\%$. Two numerical simulations were performed to account for the interaction of radiation with matter and energy deposition (Geant4), followed by ray tracing and photon propagation at the material boundaries (ZEMAX OpticStudio®).

3.1. Energy deposition

The geometry of the set-up in use for the experimental characterization has been implemented in Geant4 as shown in Fig. 12. Composite materials have been described as a single homogeneous material with densities defined as the weighted average of the chemical composition, leading to values of $4.99\,\mathrm{g/cm^3}$ for Gadox and $3.64\,\mathrm{g/cm^3}$ for YVO. The presence of the epoxy glue and the mass-ratio with the scintillating powders were both considered to set the material parameters in the simulation.

Particles have been simulated tracking the path in $10\,\mu$m steps, where for every step the direction has been smeared accounting for multiple scattering and the energy deposition has been randomly chosen according to a Landau-Vavilov distribution. The coordinates of the interaction points and the deposited energy in those points are an essential input to the optical simulation of the photon propagation. The simulation took into account the experimental conditions, namely the dimension of the specimen and the request to trigger the event relying on the pulse resulting by direct ionisation in the SiPM. The main results of the Geant4 simulation are the mean values of deposited energy ($\langle E_{dep} \rangle$), which are 0.447 MeV for the Gadox mixture and 0.342 MeV for the YVO mixture, obtained by the respective deposited energy spectra (E_{dep}). Fig. 10 shows the deposited energy spectrum for the Gadox mixture and how the trigger requirement and the system geometry influence the E_{dep} distribution.

The light blue distribution represents the deposited energy spectra in the specimen under the experimental conditions and it results by two classes of events.

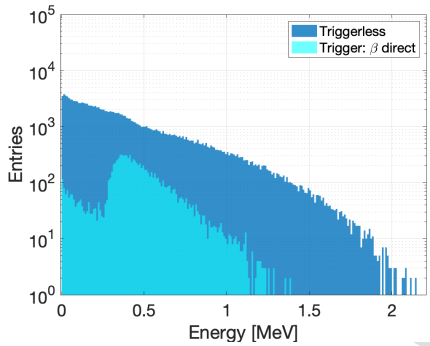

Figure 10: The ^{90}Sr E_{dep} distributions for Gadox mixture both in triggerless and in direct ionization configurations.

The first class corresponds to the β particles that cross the entire depth of the scintillator and generate a trigger in the SiPM, the second class identifies β particles that triggered the SiPM after having initially crossed the scintillator at the boundary with the PMMA disk, where they continued their path to the sensor. An exemplary distribution of the e^- traces projection on the plane at half depth of the specimen (250 μm) is shown in Fig. 11. Referring to the Gadox mixture, the generated events that have $E_{dep} < 0.27$ MeV (Fig. 11a) generally exit from the lateral surface of the specimen while events with $E_{dep} \geqslant 0.27$ MeV (Fig. 11b) cross the entire depth of the specimen and exit from the bottom face.

The series of interaction points and deposited energy obtained with the Geant4 simulation has been the base for the photon generation and tracing using ZEMAX OpticStudio®.

3.2. Photon generation and propagation

The optical characterization has shown that the materials have high absorption, therefore a large fraction of photons generated in the scintillator core remains trapped in the volume due to total internal reflection [21]. The aim of the second simulation step was to explore the effect of scintillator composition and system geometry on light collection efficiency (η), defined as the fraction

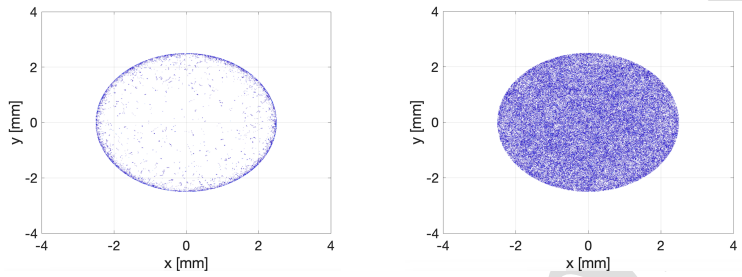

Figure 11: Distribution of the e^- traces projection on the plane at a depth of 250 μm of the Gadox specimen. If $E_{dep} < 0.27$ MeV (left) the traces are close to the border while for $E_{dep} \geqslant 0.27$ MeV the traces are uniformly distributed along the specimen plane.

of the total radiation generated by the scintillator that reaches the detector. To obtain an estimation of η, an optical simulation has been performed using ZEMAX OpticStudio®, a software designed for imaging, laser system and illumination analysis.

The simulations have been carried out in the so called "non-sequential ray tracing mode", commonly used for the analysis of non-imaging systems, where rays can propagate through optical components in any order and can be split, scatter and reflect back to an object they have already encountered.

The scintillation photons were generated isotropically in the points extracted by the Geant4 simulation and the absorption coefficient of the scintillating materials were obtained from the optical characterization of the samples. The refractive indexes of the materials were calculated as a weighted average of the single component properties ($n_{Gadox} \sim 2.0$ and $n_{YVO} \sim 1.8$) while both the refractive index of the SiPM window ($n_{SiPM} = 1.41$) and of the optical grease ($n_{grease} = 1.47$) were given by the producer. Fresnel reflection is taken into account in Zemax and a ray splits into reflected and transmitted rays when hitting a boundary of two materials.

An exemplary ray tracing of 100 rays, is shown in Fig. 12, where some rays impinge on the detector region, some other rays are trapped inside the sample

material by total internal reflection and exit from the disk side.

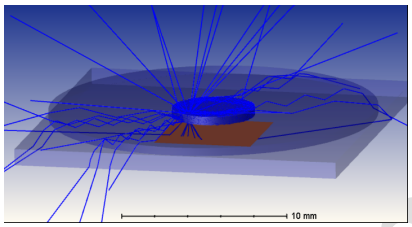

Figure 12: Set-up geometry as implemented in Geant4 and in ZEMAX OpticStudio®. The scintillating material is blue and the SiPM is red. Illustration of the ray tracing modeling of 100 rays emitted from the scintillator.

Scintillation of more than 2 million rays were modeled in Zemax for each sample. The estimated values of the light collection efficiency resulted by ZEMAX simulations are $\eta_{Gadox} = 12.75\,\%$ and $\eta_{YVO} = 8.76\,\%$. The optical simulations also allowed estimating that 81.39% of the scintillated light was absorbed in the Gadox sample, while for YVO that value was 87.05%.

3.3. Results

Once the average energy deposition is estimated by the Geant4 simulation and the fraction of escaping and detected light is computed with ZEMAX, the experimental measurements lead to the light emission per unit deposited energy in the scintillating material.

At last, the LY per unitary deposited energy was obtained as:

$$LY = \frac{LY_{eff}}{PDE(\lambda) \cdot \langle E_{dep} \rangle \cdot \eta} \tag{9}$$

Results correspond to: $\mathrm{LY}_{Gadox} = (7.1 \pm 0.5) \times 10^4$ photon/MeV and $\mathrm{LY}_{YVO} = (4.8 \pm 0.5) \times 10^4$ photon/MeV. The simulations results have been handled as devoid of errors, therefore, the error estimation on the LY values derives from the propagation of the LY_{eff} errors.

4. Conclusion

This work presents a novel procedure which allows to estimate the decay time and the absolute light output of a scintillating material exploiting the single-photon counting capability of the SiPMs. This method can be applied whenever the addressed scintillator exhibits a long decay time and a challenging identification of the photo-peaks by a γ-ray interaction.

The reported measurements correspond to a similar LY for the two materials under study, actually very high and comparable to NaI but with a useful light output strongly reduced by the extremely high internal absorption. Besides, the estimation of the decay time provides compatible results to the values reported in literature [16], [9].

5. Acknowledgements

The ORIGIN project is an initiative of the Photonics Public Private Partnership (www.photonics21.org), and has received funding from the European Union's Horizon 2020 Research and Innovation Programme under Grant Agreement n° 871324.

References

[1] P. Woulfe, F. Sullivan, W. Kam, S. O'Keeffe, Optical fiber dosimeter for real-time in-vivo dose monitoring during LDR brachytherapy, Biomedical Optics Express 11 (7) (2020) 4027–4036. doi:10.1364/BOE.385610.

[2] D. Cusumano, L. Placidi, E. D'Agostino, L. Boldrini, S. Menna, V. Valentini, M. D. Spirito, L. Azario, Characterization of an inorganic scintillator for small-field dosimetry in MR-guided radiotherapy, Journal of Applied Clinical Medical Physics 21. doi:10.1002/acm2.13012.

[3] G. Kertzscher, S. Beddar, Inorganic scintillation detectors based on Eu-activated phosphors for ^{192}Ir brachytherapy, Physics in medicine and biologydoi:10.1088/1361-6560/aa716e.

[4] G. Knoll, Radiation Detection and Measurement, 3rd Edition, John Wiley and Sons, 2000.

[5] M. Alharbi, S. Gillespie, P. Woulfe, P. McCavana, S. O'Keeffe, M. Foley, Dosimetric characterization of an inorganic optical fiber sensor for external beam radiation therapy, IEEE Sensors Journal 19 (6) (2019) 2140–2147. doi:10.1109/JSEN.2018.2885409.

[6] A. I. DeAndres, L. C. S. O'keeffe, O. Esteban, Highly sensitive extrinsic x-ray polymer optical fiber sensors based on fiber tip modification, IEEE Sensors Journal 17 (16) (2017) 5112–5117. doi:10.1109/JSEN.2017.2721105.

[7] Y. Hu, Z. Qin, Y. Ma, W. Zhao, W. Sun, D. Zhang, Z. Chen, B. Wang, H. Tian, E. Lewis, Characterization of fiber radiation dosimeters with different embedded scintillator materials for radiotherapy applications., Sensors and Actuators, A: Physical 269 (2017) 188–195. doi:10.1016/j.sna.2017.11.014.

[8] B. S. Lee, Y. M. Hwang, H. S. Cho, S. Kim, S. Cho, Fabrication of fiber-optic radiation sensor tips with inorganic scintillator for remote sensing of x or γ - ray., IEEE Nuclear Science Symposium Conference Record 2 (C) (2004) 865–868. doi:10.1109/nssmic.2004.1462344.

[9] N. Martinez, T. Teichmann, P. Molina, M. Sommer, M. S. adn J. Henniger, E. Caselli, Scintillation properties of the YVO_4:Eu^{3+} compound in powder form: Its application to dosimetry in radiation fields produced by pulsed mega-voltage photon beams., Zeitschrift Fur Medizinische Physik 25 (4) (2015) 368–374. doi:10.1109/nssmic.2004.1462344.

[10] C. Penner, P. Woulfe, B. Stoeber, C. Duzenli, S. O'Keeffe, C. Hoehr, Novel optical fibre-based sensors for neutron and proton beams., Proceedings of IEEE Sensor (2019) 1–4doi:10.1109/SENSORS43011.2019.8956683.

[11] J. de Haas, P. Dorenbos, C. van Eijk, Measuring the absolute light yield of scintillators, Nuclear Instruments and Methods in Physics Research Sec-

tion A: Accelerators, Spectrometers, Detectors and Associated Equipment 537 (1) (2005) 97–100. doi:10.1016/j.nima.2004.07.243.

[12] M. Moszynski, M. Kapusta, M. Mayhugh, D. Wolski, S. Flyckt, Absolute light output of scintillators, IEEE Transactions on Nuclear Science 44 (3) (1997) 1052–1061. doi:10.1109/23.603803.

[13] S. Sasaki, H. Tawara, K. Saito, M. Miyajima, E. Shibamura, Average energy required per scintillation photon and energy resolution in inorganic, scintillation crystals for gamma-rays, IEEE Nuclear Science Symposium Conference Record 2 (2001) 976–979. doi:10.1109/NSSMIC.2001.1009717.

[14] J. Rosado, S. Hidalgo, Characterization and modeling of crosstalk and afterpulsing in hamamatsu silicon photomultipliers, Journal of Instrumentation 10 (P10031) (2025) 1–324. doi:10.1088/1748-0221/10/10/P10031.

[15] V. Arosio, M. Beretta, M. Caccia, R. Santoro, A robust and semi-automatic procedure for silicon photomultipliers characterisation, Journal of Instrumentation 12 (C03030). doi:10.1088/1748-0221/12/03/C03030.

[16] E. Gorokhova, V. Demidenko, O. Khristich, S. Mikhrin, P. Rodnyi, Luminescence properties of ceramics based on terbium-doped gadolinium oxysulfide, Journal of Optical Technology 70 (2003) 693–698. doi:10.1364/JOT.70.000693.

[17] C. M. Lavelle, D. Raimi-Zlatic, J. Kalter, C. Chiang, T. Haard, B. Fisher, Sensitivity of silicon photomultipliers to direct gamma ray irradiation, IEEE Transactions on Nuclear Science 67 (1) (2020) 389–399. doi:10.1109/TNS.2019.2955636.

[18] J. Moyal, Theory of ionization fluctuations, Phil. Mag. Ser. 7 46 (374) (1955) 263–280. doi:10.1080/14786440308521076.

[19] T. Davidek, R. Leitner, Parametrization of the muon response in the tile calorimeter, Tech. rep., CERN, Geneva (Apr 1997).
URL http://cds.cern.ch/record/683578

[20] L. Hernandez-Adame, G. Palestino, O. Meza, P. L. Hernandez-Adame, H. R. Vega-Carrillo, I. Sarhid, Effect of tb3+ concentration in the visible emission of terbium-doped gadolinium oxysulfide microspheres, Solid State Sciences 11 (84) (2018) 8–14. doi:10.1021/acsami.9b11816.

[21] G. Keil, Design principles of fluorescence radiation converters, Nuclear Instruments and Methods 89 (1970) 111–123. doi:10.1016/0029-554X(70)90813-X.

Declaration of interests

☒ The authors declare that they have no known competing financial interests or personal relationships that could have appeared to influence the work reported in this paper.

☐ The authors declare the following financial interests/personal relationships which may be considered as potential competing interests: